Quiet Sun Magnetic Fields

Catherine E. Fischer, Kiepenheuer Institut für Sonnenphysik, Schöneckstrasse 6, 79104 Freiburg, Germany

Abstract

Time series of magnetograms showing the quiet sun expose a fascinating range of very dynamic phenomena: from magnetic flux concentrations appearing and disappearing within seconds, the dragging of magnetic flux by the fast evolving granulation flows to the accumulation of magnetic flux in the intergranular lanes and their intensification. Having sizes of only 100 km and less on the solar surface and lifetimes on the granular motion scale of minutes as well as low polarimetric signals of 10^{-3} and less, the small-scale magnetic fields are difficult to measure and interpret. Nevertheless, using high-resolution observations and probing the solar atmosphere at multiple heights simultaneously, different aspects of the small-scale magnetic field have been revealed. These discoveries have been aided by the comparison with sophisticated numerical simulations that reproduce the observations. In this review, I will highlight some of the results concerning the small-scale magnetic field origin, distribution, evolution and destruction and identify current open questions.

1. Introduction

Magnetic fields pervade the universe at all scales and the polarization signals signifying magnetic fields reach us from distant galaxies, the interstellar medium itself, to our closest star, the sun. The magnetic fields on the sun are the principal ingredient causing solar irradiance variability measured on earth (Solanki & Fligge 2002), the velocity distribution in the solar wind permeating the entire solar system (Weber & Davis 1967) and the impulsive solar surface explosions whose effects impact earth as impressively demonstrated in the "Bastille Day" solar flare in 2000.

Figure 1 (left) shows the longitudinal magnetic field for the visible solar surface and, on the right, for a small subfield of 150 arcsec to 150 arcsec. One can clearly see how the solar surface is penetrated by the small-scale magnetic field forming an omnipresent magnetic carpet. We know that upwards, the field rises through the photosphere and expands and extends through the chromosphere up into the corona. In the lower solar atmosphere, at the surface, the violently "bubbling" granulation with its strong flows tosses the frozen magnetic field seemingly arbitrarily around. This has consequences higher up, where the magnetic field dominates over the unmagnetized gas, leading to the large variety of observed dynamic processes. Now it is believed that it is this interplay that is responsible for the heating of the solar chromosphere and corona, one of the most persistent mysteries in solar physics. Small-scale magnetic fields have moved into the limelight in the last decades as they are suspected to be a main

contributor in this process. Consequently, a hot debate on their nature and their rapid and dynamic evolution has emerged as reviewed for example by de Wijn et al. (2009).

It is an instrumental challenge to measure the weak signal formed in the magnetized atmosphere, smeared by the nature of their rapid evolution, the limited spatial resolution obtained and, in case of the ground-based telescopes also the turbulent earth atmosphere. And therefore, despite spectacular advances that have been made over the past decade in solar instrumentation and analysis techniques, fundamental questions remain:

➢ What is the distribution of the magnetic field in the quiet sun?
➢ How is the small-scale magnetic field created?
➢ How do the magnetic elements interact with the non-magnetized plasma and what are the effects on the solar atmosphere from the photosphere to the corona?
➢ What is the physical process that destroys magnetic flux?

Figure 2 (left) shows a cartoon of a possible topology of the small-scale magnetic fields embedded in the solar surface granulation. Depending on the observational methods, a different population of magnetic fields – weak internetwork, strong kiloGauss (kG) flux tubes, turbulent fields – is revealed. In addition, these magnetic structures are highly interactive with the surrounding non-magnetized gas. These dynamic processes
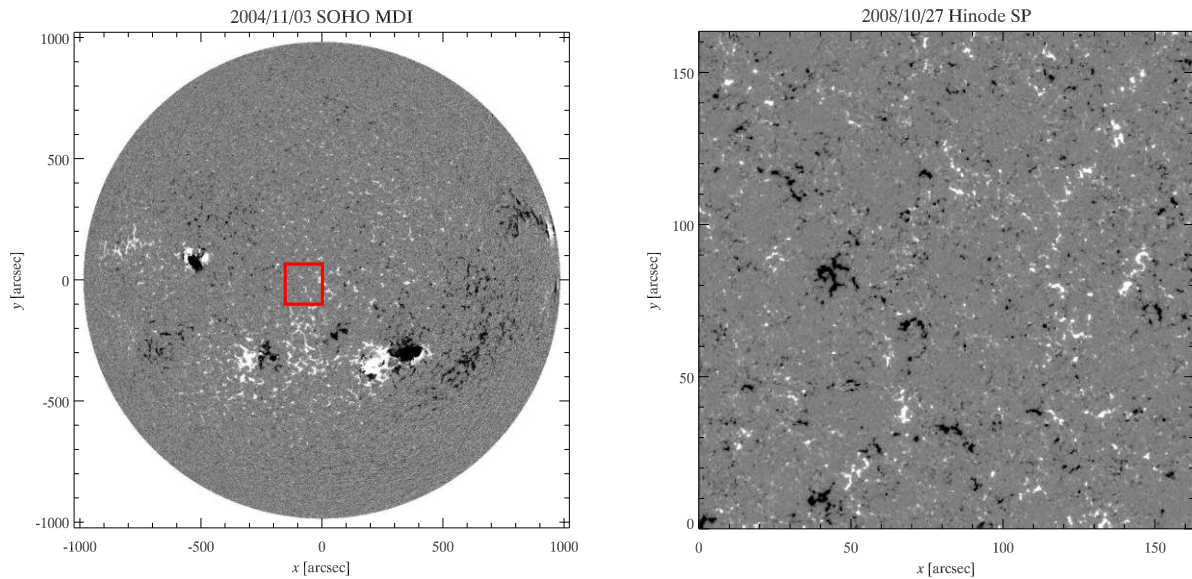
Figure 1: Magnetic map of the photosphere. White patches denote magnetic flux pointing toward the viewer and black patches point in the opposite direction. Left: The full disk magnetogram was recorded by the Michelson Doppler Imager (MDI) on the SOlar and Heliospheric Satellite (SOHO, Fleck et al. 1995). The red box demonstrates the size of the right image (not co-temporal) in respect to the full disk. Right: Quiet sun longitudinal magnetogram obtained with the Spectropolarimeter of the Hinode satellite. Image and caption from Fischer (2011).

processes are multi-dimensionally interrelated and not confined to the window we are restricted to when observing in a spectral line with a limited formation height. As one can see in Fig. 2 (right) the magnetic structures appear very differently at the different observed wavelengths revealing the complexity of the magnetic structures.

In the next section, I will briefly introduce some of the measurement techniques used to infer properties of the small-scale magnetic fields before showcasing some of the results obtained in the last decades of studying the small-scale magnetic field.

## 2. Quantifying the small-scale magnetic fields

Images taken in the continuum of a spectral line and in e.g. the G-band (passband at 430 nm) exhibit the familiar granulation pattern of the photosphere. In the dark lanes one can see bright points which gather, are pushed around, and disappear on granular timescales coinciding with magnetic elements seen for example in co-temporal magnetograms. Corresponding bright points are also observed in, for example, Ca II H images.

These bright points have been used as proxies for magnetic elements and utilized to determine their characteristics such as their lifetime, size and apparent horizontal velocities (see e.g. Abramenko et al. 2010). The advantage of this proxy-magnetometry as a purely imaging method is, that one can scan very fast at high resolution. Although these brightenings have been well explained for the G-band (Rutten et al. 2001) the connection between the brightening seen in e.g. Ca II H

and the underlying magnetic elements is not yet completely understood. It is also not yet clear, if the brightenings are produced by strong magnetic fields or even weaker fields as demonstrated by, for example, Criscuoli & Uitenbroek (2014) and therefore this approach does not allow for conclusions on the type of the magnetic field population encountered.

As one cannot measure the magnetic field directly on the sun, one is confined to study the imprint the atmospheric conditions have left on the spectrum that reaches the observer. Especially, knowledge of the polarization state of the light is utilized to learn about the magnetized solar atmosphere. There have been several reviews on polarization measurements and their role in inferring the magnetic field vector on the sun (e.g. Lagg et al. 2015). Here, I will limit myself to briefly mention the methods employed and point out their advantages and drawbacks when coupled with the instrumental challenges one faces.

The Zeeman effect has provided us with a powerful tool in inferring the magnetic field vector from polarization measurements on the sun. Due to the presence of a magnetic field, the atomic energy levels, previously degenerate, split into several components shifted in energy - consequently resulting in wavelength shifts for the emitted light caused by transitions between the energy levels. This light is, in addition, polarized and by measuring the polarization state of the incoming light, we can deduce the magnetic field vector. It turns out to be very useful to use the Stokes vector (I,Q,U,V) obtained by differential measurements, to describe the polarization properties of the incoming light and the Muller matrix formalism to describe the effects of
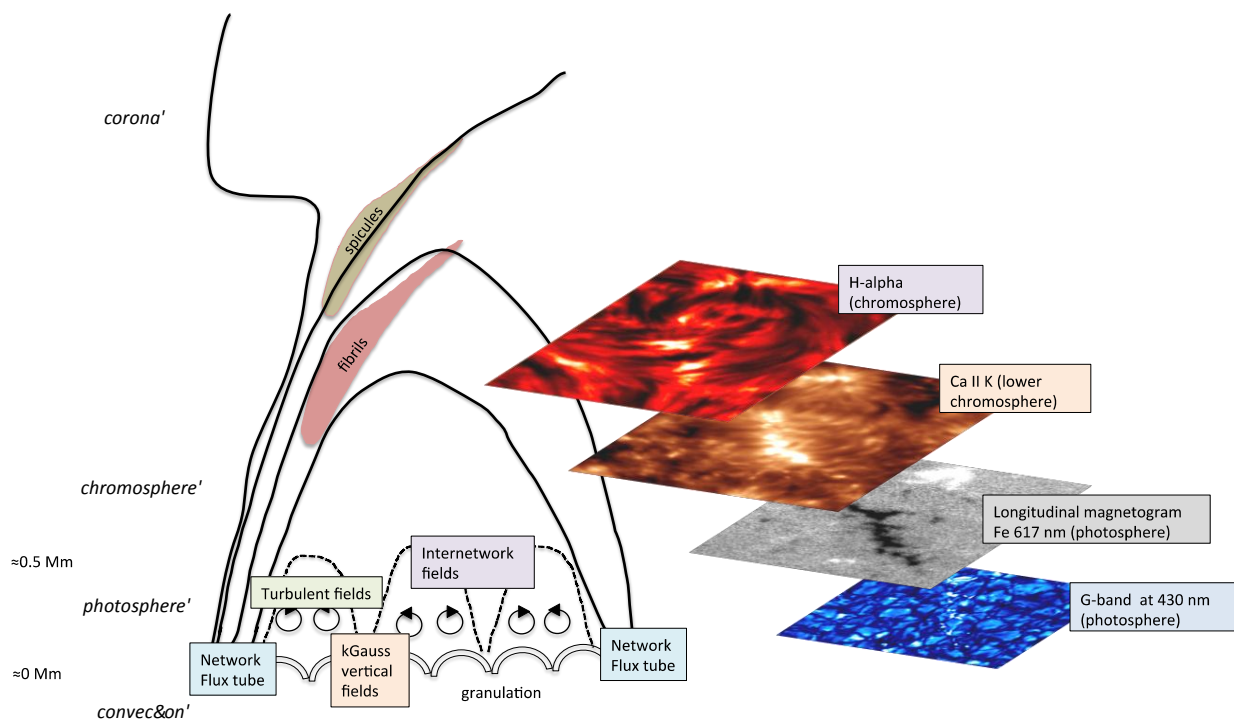
Figure 2: Left: Quiet sun magnetic field topology based on a variety of observational evidence. Strong magnetic flux tubes placed in the intergranular lane form the network. Black lines denote magnetic field. Spicules are hot gas ejected into the chromosphere. Fibrils are observed as dark elongated patches on disk, for example, in Hα. The weaker internetwork magnetic field forms a carpet of low-lying magnetic loops. The turbulent magnetic field covers the entire surface in this model. Right: Same field of view of approximately 40 arcsec to 60 arcsec taken at different wavelengths with the IBIS (Cavallini 2006) instrument at the Dunn Solar Telescope. From bottom up: G-band at 430 nm, longitudinal magnetic flux in Fe I 617.3 nm with dark and bright patches denoting opposite magnetic flux, Ca II K and Hα intensity images.

optical elements on the Stokes vector. The wavelength dependent Stokes I shows the intensity spectrum of the spectral line, whereas the symmetric Q and U signals denote linear polarization and the anti-symmetric Stokes V quantifies the circular polarization. Their relation to the magnetic field vector direction depends on the line-of-sight of the observer. Observing at disk center, the Stokes Q and U signals relay information on the transversal magnetic field and the Stokes V signal reveals the magnetic field component pointing towards or opposite to the observer. There is a natural 180 disambiguity in the magnetic field azimuth of the transversal field that cannot be resolved with the Zeeman effect even when employing the ideal instrument.

A longitudinal field magnetograph collects the circular polarization signal in the wing of a spectral line. For weak fields, the amplitude of the signal is proportional to the magnetic field strength and for strong magnetic fields, the increase of the polarization continues, however, less noticeable as the Stokes V lobes drift apart due to the increasing magnetic field strength.

In an ideal case, one would obtain the complete information (besides the 180 degree ambiguity) of the magnetic field vector when measuring the Stokes vector arising from a non-evolving, resolved magnetic element at a defined formation height with resolved spectral

resolution. In reality, there is a spatial, temporal and spectral smearing worsened by the fact that the height of formation of lines is not well defined and often not known as well as the fact that the polarization signals are low (polarization signals at a few 10^{-3} or less in the internetwork). This poses a challenge to the instrumental design, the drafting of an observing program and the interpretation of the data.

For example, not resolving the magnetic elements leads, at disk center, to (1) cancelation in the Stokes V signals of opposite polarity magnetic elements and thus, misleading the interpretation of the observed signal to (2) abnormal shaped profiles if the elements exhibit differing line-of-sight velocities. These complex Stokes profiles can also result from gradients of the atmospheric parameters along the line-of-sight. Socas-Navarro & Sánchez Almeida (2003) show that the contradicting findings in the visible and the infrared which suggest different magnetic field population can be explained by the differing formation height of the lines.

Computerized fitting codes with many degrees of freedom employing guess models for the solar atmosphere, so-called Stokes Inversion codes (see Ruiz Cobo & del Toro Iniesta 1992), have been created to tackle the formidable task of extracting the
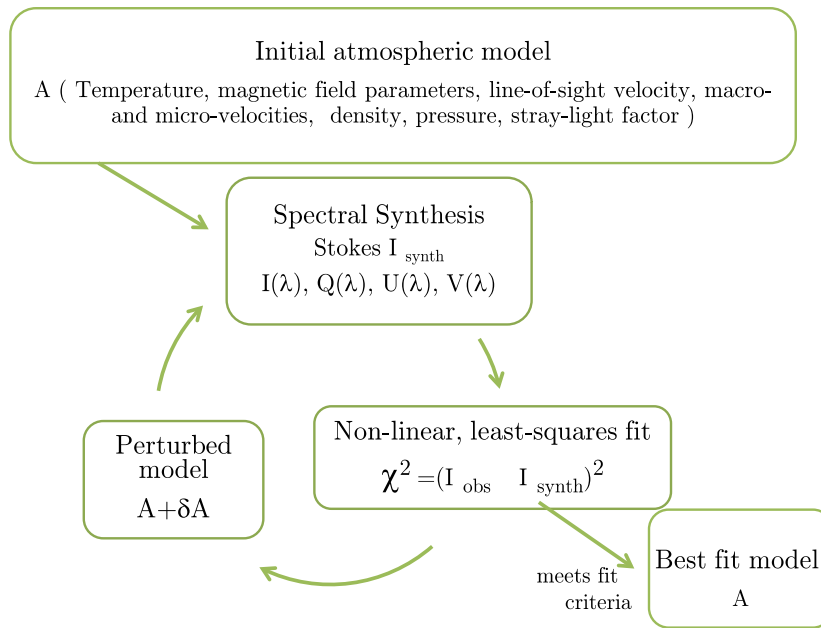
Figure 3: Schematic view of the Stokes Inversion process. I_{synth} and I_{obs} refer to the synthetic profiles $(I(\lambda), Q(\lambda), U(\lambda), V(\lambda))$, obtained by forward modeling employing the initial guess atmospheric model A, and to the observed profiles $(I(\lambda), Q(\lambda), U(\lambda), V(\lambda))$, respectivly.

atmospheric parameters such as temperature, magnetic field vector and velocities from the often observed weak signals. The general Stokes Inversion scheme is shown in Figure 3. Whereas Milne-Eddington codes (e.g. MERLIN, Lites 2007; MELANIE, Socas-Navarro 2001) limit themselves to constant parameters in, e.g. the magnetic field strength, inclination and azimuth − thereby giving a sort of average atmosphere along the line-of-sight −, height-dependent codes try to extract as much information as possible by allowing for gradients in the solar atmospheric models (LILIA, Socas-Navarro 2001; SIR, Ruiz Cobo & del Toro Iniesta 1992). Some codes offer the option to use several magnetic components to more realistically represent the multicomponent magnetic population contained in the spatial sampling pixel (see the various incarnations of the SIR code).

In Stenflo & Keller (1996), a richly structured linear polarization signature observed for many spectral lines and caused by scattering was discussed as a new diagnostic window giving rise to its own name, the so-called "Second Solar Spectrum". Scattering polarization is caused by asymmetries in the illumination in the solar layers (Manso Sainz et al. 2004). In a magnetized atmosphere, the scattered polarized light changes amplitude and direction. This so-called Hanle effect is a complementary diagnostic tool to the Zeeman effect, since opposite signs of magnetic fields do not cancel out, and is sensitive to fields of approximately 0.001 to around 100 Gauss. However, due to the even weaker polarization signals (order of 10^{-4}) in comparison to the signals owing to the Zeeman effect, measurements of

scattering polarization are rare. Another obstacle is, that the scattering polarization signals are largest at the solar limb, where the adaptive optics systems, designed to counteract the atmospheric turbulence in ground based observations, have difficulties to perform well. In addition, the shapes of the linear polarization profiles of the scattering polarization lines are often intricate and evolve fast. A vast apparatus of theoretical models have been developed to investigate the complicated and enigmatic signals and progress is being made by constraining the theoretical models with observational data.

The following sections outline the debates currently at the forefront of quiet sun magnetic field studies.

3. Small-scale magnetic field population

It was long believed that strong kiloGauss flux tubes were the dominant factor in the internetwork small-scale magnetic field population (Stenflo 1973). They are thought to be mainly vertical, occupying only a fraction of the current resolution elements and residing in the intergranular lanes. Lites et al. (2008), thanks to the high polarimetric sensitivity of the Hinode mission (Kosugi et al. 2007), found a universal population of patches of horizontal magnetic flux in the quiet sun internetwork. An ubiquitous, nearly horizontal magnetic field component in the quiet sun had been discovered before by Harvey et al. (2007), but it was the findings of Lites et al. (2008) which placed a new importance

on the transverse magnetic field as they found a stronger spatially averaged transverse magnetic flux compared to the spatially averaged longitudinal magnetic flux. A new picture of the small-scale internetwork magnetic field emerged with the horizontal field playing the key role. Orozco Suárez et al. (2007) used a Milne-Eddington inversion code to deduce the magnetic field orientations from the same Hinode data. Their results supported the findings of Lites et al. (2008), which further fueled the debate about the true nature of small-scale solar magnetic fields. Others concluded a mixture of strong kG magnetic fields in the intergranular lanes surrounded by a sea of weaker isotropically distributed magnetic fields (Stenflo 2011).

All the aforementioned observations were based on the Zeeman effect which has been invaluable in understanding the wide spectrum of magnetic processes on the sun. However, as described in section 2, due to the cancelation of mixed polarities in a single resolution element, it is effectively blind to turbulent magnetic fields. This is where one turns to the Hanle effect. Trujillo Bueno et al. (2004), investigating in the Sr I 460.7 nm line employing the Hanle effect, revealed yet another aspect of the small-scale magnetic field. They discovered, combining their observations with modeling, a turbulent field with a mean strength of 130 Gauss. The horizontal fields from the Hinode studies could be the same magnetic field population, but only partially detected through the eyes of the Zeeman effect as pointed out in Bellot Rubio & Orozco Suárez (2012).

The final answer is not yet out on the question of magnetic field population and publications such as the finding from Borrero & Kobel (2011) have demonstrated that the tools used in inferring the magnetic fields are sensitive to the photon noise and the selection criteria used by the observers so that only with an increase in resolution and polarimetric sensitivity we have hope of settling this debate.

4. Small-scale magnetic field origin

Another hint as to the small-scale magnetic field distribution might be found by determining its origin. Is the small-scale magnetic field simply the end product of active region remnants, are we seeing pre- dominantly emerging flux boiling up from the convection zone as observed by Centeno et al. (2007)? Or is it produced right there in the highest layer of the convection zone very close to the photosphere by a local dynamo action as suggested by the 3D magnetohydrodynamic simulations by Vögler & Schüssler (2007)? Martínez González & Bellot Rubio (2009) have found in their quiet sun study a rate of 0.02 for magnetic Ω–loop emergence per hour and arcsec squared contributing significantly to the internetwork magnetic population. In Martínez González et al. (2012) they further show that the emerging loops do not appear uniformly on the solar surface. They observe "calm" regions, showing only weak magnetic field signal and argue that it is unlikely that this large scale organization is a product of the random walk of active region remnants. Showing that there is no magnetic flux imbalance (Lites 2011) and no long-time variation in horizontal magnetic fields (Buehler et al. 2013), the support for a local dynamo is growing. In addition, Danilovic et al. (2010) showed, when using a scaling factor for the magnetic field, a consistency between synthesized data from local dynamo simulations and observations. Another strong argument in favor or against a local dynamo would be the direct observation of the spatial structure of the weak turbulent field on a much smaller − the granular − scale. The weak turbulent magnetic field, due to its tangled nature, is a natural candidate for a signature of the small-scale dynamo. One would expect the scattering polarization to differ in magnitude between the granular and intergranular lanes as the strongest of the weak turbulent magnetic fields are believed to be hosted within the intergranules. Comparing high-resolution observations categorizing the scattering polarization and depolarization effects with local dynamo simulation results is crucial in clarifying this issue.

5. Small-scale magnetic field dynamics

By equating the known kinetic energy density of the convective flows with the magnetic energy density in the photosphere one reaches an equipartition field strength of ≈ 500 G (Takeuchi 1999). This is however significantly less than inferred from the measurements of Stenflo (1973), who found strong kG magnetic flux tubes residing in intergranular lanes (see section 4). Parker (1978) suggested the so-called convective collapse process, where a magnetic flux tube seated in the intergranular lane is exposed to a strong downdraft evacuating the tube. To restore equilibrium between the inner tube atmosphere and the outer pressure field, the magnetic field − and therefore the magnetic pressure − in the tube increases, leading to the observed kG flux tubes. Indirect observational confirmation of this process was obtained by e.g., Bellot Rubio et al. (2001), but it was not until the high-resolution data from Hinode became available, that Nagata et al. (2008) finally delivered the first direct observational evidence of the convective collapse process by tracing an event in the photosphere and in Ca II H images.

A statistical study of convective collapse events was published in Fischer et al. (2009) where it was demonstrated that the convective collapse process occurs frequently in the quiet sun. Figure 4 shows such an observed event seen in the analyzed Hinode data.

Once formed, the strong magnetic elements are still subject to the convective granulation flows and p-mode oscillations − the 5 minute oscillations
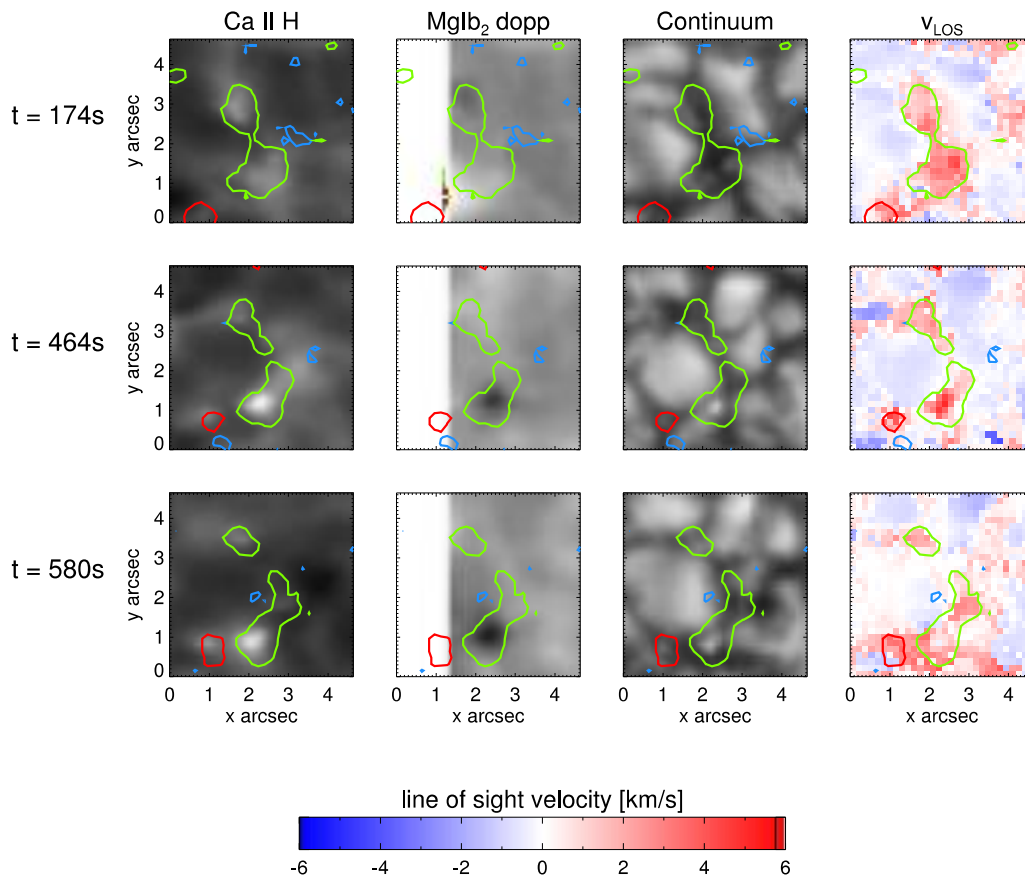
Figure 4: A convective collapse event associated with downflows in the upper photosphere observed with Hinode. The columns show the Ca II H intensity (linear scale), the magnesium dopplergram in arbitrary units (black corresponds to downflows), the continuum intensity in a linear scale, and the line-of-sight velocity derived through inversion of the Fe I 630 nm line profiles, with positive values corresponding to downflows. Green and red contours indicate the location of line-of-sight opposite polarity magnetic flux. The contour levels are at ±30Mx/cm2 in the apparent longitudinal flux density. The blue contours indicate the transverse apparent flux density at 140 Mx/cm2. Figure and caption from Fischer et al. (2009).

observed on the entire solar surface – and stay far from stable. An unexplained oscillatory pattern in the chromospheric filtergram intensities, magnetic field strength and photospheric velocity flows was in addition found in Fischer et al. (2009). This could be perhaps the signature of propagating magneto-acoustic waves (Jess et al. 2012) such as the high energetic acoustic waves detected by Bello González et al. (2010).

Small-scale jets, called spicules when observed at the solar limb, are continuously propelled into the higher atmosphere within minutes. These jets are omnipresent on the solar disk, seem to be associated to magnetic field elements and expel material carrying about 100 times the mass of the solar wind at apparent velocities of around 50km/s to 100km/s into the corona (De Pontieu et al. 2011). In addition, spicules are thought to be responsible for the energy coupling and energy transport from the solar photosphere towards the upper corona by means of magnetohydrodynamic (MHD) waves. These waves may induce the oscillatory phenomena frequently detected in limb spicules. As

reported by Zaqarashvili & Erdélyi (2009), they are frequently interpreted as (1) kink waves propagating along thin magnetic flux tubes – where spicules are formed on field lines –, causing the transverse oscillations of spicules, (2) Alfvén waves propagating in spicules surroundings, resulting in the oscillation of the ubiquitous magnetic field lines, or (3) transverse pulses excited in the photospheric magnetic flux tube by the convecting buffeting of granules. Yet, despite these various theories suggesting their origin, see e.g. Sterling (2000) and Tsiropoula et al. (2012) for an overview, their physical properties and formation are still not fully understood.

In Bello González et al. (2010), the investigation of oscillatory phenomena in the quiet magnetic sun from IMaX/SUNRISE (Solanki et al. 2010) data revealed that acoustic power of periods less than ≈100s carry at least half of the flux needed to balance the observed radiative energy losses of the quiet chromo- sphere according to Anderson & Athay (1989). The main contribution to the acoustic energy flux was
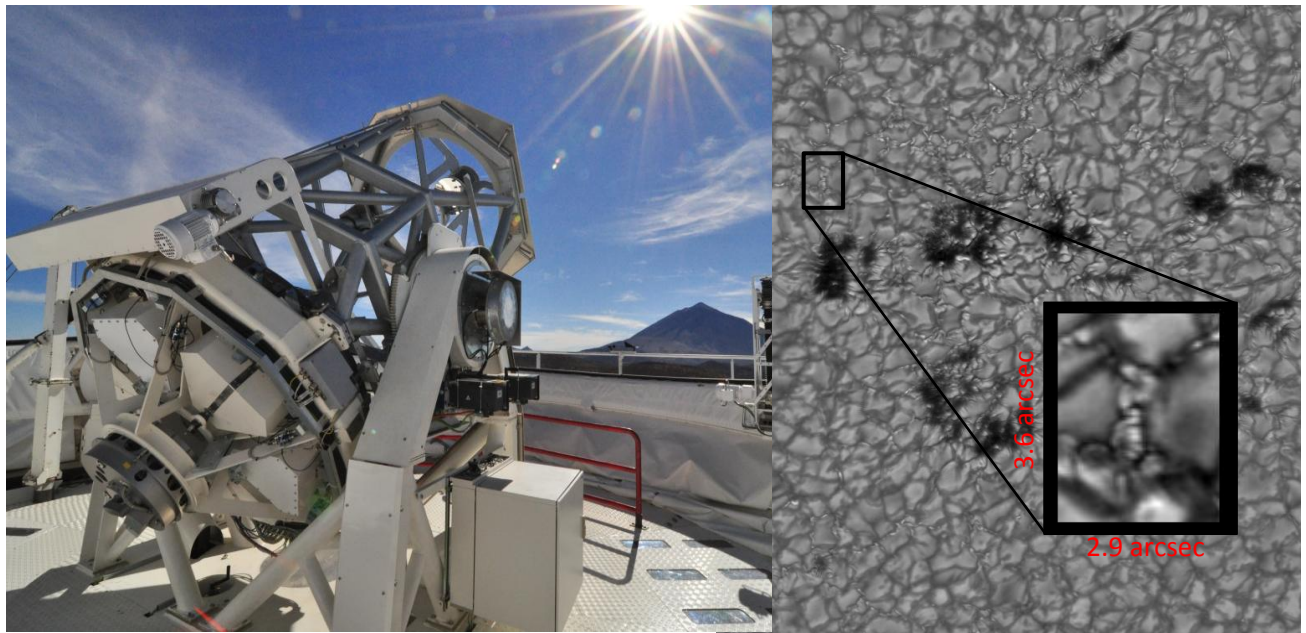
Figure 5: Left: GREGOR telescope at the Teide Observatory on Tenerife (courtesy of Dr. H.-P. Doerr). Right: One of the first images of the Broad-Band Imager at the GREGOR telescope at 486nm (courtesy of Dr. R. Schlichenmaier for the GREGOR team).

mainly found in intergranules, as is extensively known. Yet, dark dots and lanes above splitting granules and bright granular borders were found to equally be sources of propagating waves. As a biproduct of this analysis, intermittent sources of strong energy fluxes at all frequencies in the acoustic domain showed to have diverse origin; such as magnetic monopoles, magnetic bipoles and non-magnetized jets of material.

6. Small-scale magnetic field cancelation and reconnection

Schrijver et al. (1997) estimated from Michelson Doppler Imager (MDI) photospheric magnetograms that flux cancelation occurs at a rate of 3×10^{21} Mx/hr for the total solar surface. They observed the merging of opposite-polarity magnetic elements that had been advected toward each other and the consecutive disappearance of one or both magnetic elements.

According to Zwaan (1987), there are three ways to remove magnetic flux from the solar surface. The first configuration is a simple retraction with an opposite-polarity pair connected through a loop being dragged into the convection zone without any reconnection taking place. The observational signature on the photosphere is two opposite polarities, followed by a short transverse magnetic field signal when the loop top passes the solar surface. In the second and third scenario the opposite polarities are at first not connected. They are convectively forced together and reconnection takes place either above or below the solar surface. In both cases two new loops have formed. In the case of reconnection below the surface the newly formed U-loop travels upward, causing a transverse magnetic field

signal when passing the surface. Whereas, if reconnection takes place above the photosphere, an Ω-loop is formed and consequently submerges. The observational signature at the solar surface is for all three cases the same, and one can not distinguish between these cases without additional, height-dependent information.

Harvey et al. (1999) studied chromospheric magnetograms in addition to photospheric magnetograms. They showed that in most cases the chromospheric magnetic flux disappeared earlier than the photospheric magnetic flux and suggested that reconnection takes place primarily above the photosphere with subsequent submergence of Ω-loops. However, their data were taken with moderate spatial resolution of one to two arcsec and a low cadence around 7 minutes. The spatial resolution and polarimetric sensitivity becomes crucial when comparing disappearance or appearance of magnetic structures at different solar layers. There have been several studies utilising high-resolution spectropolarimetric data analysing the velocity and magnetic field associated with cancelation events, with some reporting downflows (Iida et al. 2010) and others additional upflows during the cancelation event (e.g., Kubo & Shimizu 2007) or even supersonic upflows (Borrero et al. 2010). Explosive events found in EUV data from the SDO satellite (Pesnell et al. 2012) seem to be connected to flux cancelation sites (Innes & Teriaca 2013).

However, the role of reconnection and the height at which it predominantly occurs have not been identified. Kubo et al. (2014) demonstrated effectively, using high resolution Hinode spectropolarimeter data, that, by

combining Stokes V profiles taken from both interacting polarities during the cancelation process, the complex profiles shapes
(previously explained by the reconnection process) could be reproduced at the polarity inversion line. We therefore currently might not have the necessary spatial resolution to directly observe and characterize the cancelation process.

7. Outlook

The next years will prove very rewarding with the GREGOR (Volkmer et al. 2010) and NST (New Solar Telescope, Goode et al. 2010) telescopes reaching maturity and the Daniel K. Inouye Solar Telescope approaching its first-light date (*http://dkist.nso.edu/*). We can expect a flood of high-resolution polarimetric data expanding our knowledge of the dynamic small-scale magnetic elements. Furthermore, the availability of more powerful supercomputers enables to perform ever more realistic time-dependent MHD simulations. The relationship between theoretical simulations and observations is symbiotic in the sense that one can foster and enhance the other and vice-versa which make them a unique and helpful tool.
Finally, studying the small-scale magnetic fields does not only expand our knowledge of basic physical processes on a subarcsec scale, but understanding their origin and evolution will also shed light on the large scale development of the global magnetic field.

Literature

Abramenko, V., Yurchyshyn, V., Goode, P., & Kilcik, A., 2010, ApJ, 725, L101
Anderson, L. S. & Athay, R. G. 1989, ApJ, 346, 1010
Bello González, N., Flores Soriano, M., Kneer, F., Okunev, O., & Shchukina, N. 2010, A&A, 522, A31
Bellot Rubio, L. R. & Orozco Suárez, D. 2012, ApJ, 757, 19
Bellot Rubio, L. R., Rodríguez Hidalgo, I., Collados, M., Khomenko, E., & Ruiz Cobo, B. 2001, ApJ, 560, 1010
Borrero, J. M. & Kobel, P. 2011, A&A, 527, A29
Borrero, J. M., Martínez-Pillet, V., Schlichenmaier, R., et al. 2010, ApJ, 723, L144
Buehler, D., Lagg, A., & Solanki, S. K. 2013, A&A, 555, A33
Cavallini, F. 2006, Sol.Phys., 236, 415
Centeno, R., Socas-Navarro, H., Lites, B., et al. 2007, ApJ, 666, L137
Criscuoli, S. & Uitenbroek, H. 2014, A&A, 562, L1
Danilovic, S., Schüssler, M., & Solanki, S. K. 2010, A&A, 513, A1

De Pontieu, B., McIntosh, S. W., Carlsson, M., et al. 2011, Science, 331, 55
de Wijn, A. G., Stenflo, J. O., Solanki, S. K., & Tsuneta, S. 2009, Space Science Rev., 144, 275
Fischer, C. E. 2011, PhD thesis, Universiteit Utrecht, The Netherlands
Fischer, C. E., de Wijn, A. G., Centeno, R., Lites, B. W., & Keller, C. U. 2009, A&A, 504, 583
Fleck, B., Domingo, V., & Poland, A. I. 1995, Sol.Phys., 162
Goode, P. R., Coulter, R., Gorceix, N., Yurchyshyn, V., & Cao, W. 2010, Astronomische Nachrichten, 331, 620
Harvey, J. W., Branston, D., Henney, C. J., Keller, C. U., & SOLIS and GONG Teams. 2007, ApJ, 659, L177
Harvey, K. L., Jones, H. P., Schrijver, C. J., & Penn, M. J. 1999, Sol.Phys., 190, 35
Iida, Y., Yokoyama, T., & Ichimoto, K. 2010, ApJ, 713, 325
Innes, D. E. & Teriaca, L. 2013, Sol.Phys., 282, 453
Jess, D. B., Shelyag, S., Mathioudakis, M., et al. 2012, ApJ, 746, 183
Kosugi, T., Matsuzaki, K., Sakao, T., et al. 2007, Sol.Phys., 243, 3
Kubo, M., Chye Low, B., & Lites, B. W. 2014, ApJ, 793, L9
Kubo, M. & Shimizu, T. 2007, ApJ, 671, 990
Lagg, A., Lites, B., Harvey, J., Gosain, S., & Centeno, R. 2015, Space Science Rev.
Lites, B., Casini, R., Garcia, J., & Socas-Navarro, H. 2007, Mem. Soc. Astron. Italiana, 78, 148
Lites, B. W. 2011, ApJ, 737, 52
Lites, B. W., Kubo, M., Socas-Navarro, H., et al. 2008, ApJ, 672, 1237
Manso Sainz, R., Landi Degl'Innocenti, E., & Trujillo Bueno, J. 2004, ApJ, 614, L89
Martínez González, M. J. & Bellot Rubio, L. R. 2009, ApJ, 700, 1391
Martínez González, M. J., Manso Sainz, R., Asensio Ramos, A., & Hijano, E. 2012, ApJ, 755, 175
Nagata, S., Tsuneta, S., Suematsu, Y., et al. 2008, ApJ, 677, L145
Orozco Suárez, D., Bellot Rubio, L. R., del Toro Iniesta, J. C., et al. 2007, ApJ, 670, L61
Parker, E. N. 1978, ApJ, 221, 368
Pesnell, W. D., Thompson, B. J., & Chamberlin, P. C. 2012, Sol.Phys., 275, 3
Ruiz Cobo, B. & del Toro Iniesta, J. C. 1992, ApJ, 398, 375
Rutten, R. J., Kiselman, D., Rouppe van der Voort, L., & Plez, B. 2001, in ASPC Series, Vol. 236, Advanced Solar Polarimetry – Theory, Observation, and Instrumentation, ed. M. Sigwarth, 445
Schrijver, C. J., Title, A. M., van Ballegooijen, A. A., Hagenaar, H. J., & Shine, R. A. 1997, ApJ, 487, 424
Socas-Navarro, H. 2001, in ASPC Series, Vol. 236, Advanced Solar Polarimetry – Theory, Observation, and Instrumentation, ed. M. Sigwarth, 487
Socas-Navarro, H. & Sánchez Almeida, J. 2003, ApJ, 593, 581
Solanki, S. K., Barthol, P., Danilovic, S., et al. 2010, ApJ, 723, L127
Solanki, S. K. & Fligge, M. 2002, Advances in Space Research, 29, 1933
Stenflo, J. O. 1973, Sol.Phys., 32, 41
Stenflo, J. O. 1996, Nature, 382, 588
Stenflo, J. O. 2011, A&A, 529, A42
Sterling, A. C. 2000, Sol.Phys., 196, 79
Takeuchi, A. 1999, ApJ, 522, 518
Trujillo Bueno, J., Shchukina, N., & Asensio Ramos, A. 2004, Nature, 430, 326
Tsiropoula, G., Tziotziou, K., Kontogiannis, I., et al. 2012, Space Science Rev., 169, 181
Vögler, A. & Schüssler, M. 2007, A&A, 465, L43
Volkmer, R., von der Lühe, O., Denker, C., et al. 2010, Astronomische Nachrichten, 331, 624
Weber, E. J. & Davis, Jr., L. 1967, ApJ, 148, 217
Zaqarashvili, T. V. & Erdélyi, R. 2009, Space Science Rev., 149, 355
Zwaan, C. 1987, ARA&A, 25, 83